

Feedback Effects of Sediment Suspensions on Transport Mechanisms in an Estuarine Turbidity Maximum

Zhu, Chunyan; van Maren, D. S.; Guo, Leicheng; Lin, Jianliang; He, Qing; Wang, Zheng Bing

DOI

[10.1029/2021JC018029](https://doi.org/10.1029/2021JC018029)

Publication date

2022

Document Version

Final published version

Published in

Journal of Geophysical Research: Oceans

Citation (APA)

Zhu, C., van Maren, D. S., Guo, L., Lin, J., He, Q., & Wang, Z. B. (2022). Feedback Effects of Sediment Suspensions on Transport Mechanisms in an Estuarine Turbidity Maximum. *Journal of Geophysical Research: Oceans*, 127(6), Article e2021JC018029. <https://doi.org/10.1029/2021JC018029>

Important note

To cite this publication, please use the final published version (if applicable). Please check the document version above.

Copyright

Other than for strictly personal use, it is not permitted to download, forward or distribute the text or part of it, without the consent of the author(s) and/or copyright holder(s), unless the work is under an open content license such as Creative Commons.

Takedown policy

Please contact us and provide details if you believe this document breaches copyrights. We will remove access to the work immediately and investigate your claim.





Green Open Access added to TU Delft Institutional Repository

'You share, we take care!' - Taverne project

<https://www.openaccess.nl/en/you-share-we-take-care>

Otherwise as indicated in the copyright section: the publisher is the copyright holder of this work and the author uses the Dutch legislation to make this work public.

Feedback Effects of Sediment Suspensions on Transport Mechanisms in an Estuarine Turbidity Maximum

Chunyan Zhu^{1,2} , D. S. van Maren^{1,2,3}, Leicheng Guo¹ , Jianliang Lin^{1,2}, Qing He¹ , and Zheng Bing Wang^{1,2,3} 

¹State Key Lab of Estuarine and Coastal Research, East China Normal University, Shanghai, China, ²Faculty of Civil Engineering and Geosciences, Delft University of Technology, Delft, The Netherlands, ³Deltares, Delft, The Netherlands

Key Points:

- Sediment trapping due to tidal flood dominance can be weakened by Sediment-induced density effects (SedDE)
- With SedDE, high water (HW) slack tide asymmetry favors landward migration of the sediment trapping location
- Higher near-bed suspended sediment concentrations/suspended sediment concentration strengthens the role of estuarine circulation in sediment trapping in estuaries with strong river and tidal flow

Supporting Information:

Supporting Information may be found in the online version of this article.

Correspondence to:

Q. He,
qinghe@sklec.ecnu.edu.cn

Citation:

Zhu, C., van Maren, D. S., Guo, L., Lin, J., He, Q., & Wang, Z. B. (2022). Feedback effects of sediment suspensions on transport mechanisms in an estuarine turbidity maximum. *Journal of Geophysical Research: Oceans*, 127, e2021JC018029. <https://doi.org/10.1029/2021JC018029>

Received 22 SEP 2021

Accepted 6 MAY 2022

Abstract The mechanisms controlling the formation of an estuarine turbidity maximum (ETM) in estuaries have been extensively investigated, but one aspect that has received much less scientific attention is the role of high suspended sediment concentrations in combination with tidal asymmetry in ETM formation. Particularly in highly turbid estuaries, sediment suspensions influence ETM development through a combination of horizontal sediment-induced density currents, a reduction in turbulent mixing, and water-bed exchange processes. In this study, we developed a schematic model resembling the Yangtze Estuary where the ETM is controlled by tidal pumping, estuarine circulation, and advection operating simultaneously. Model results suggest that high water slack tide asymmetry with Sediment-induced density effects (SedDE) favors landward migration of the ETM. In addition, without SedDE, stronger flood tidal dominance leads to more pronounced sediment trapping through tidal pumping. Depending on the type of tidal asymmetry, SedDE strengthen ETM growth by increasing estuarine circulation but may also lead to increased or reduced sediment concentration in the ETM due to enhanced or weakened landward tidal pumping, respectively. Higher near-bed sediment concentrations as a result of water-bed exchange processes, in turn, strengthen the effect of estuarine circulation but simultaneously strengthen the divergence of sediment by tidal pumping. Overall, the SedDE and higher near-bed sediment concentration, in combination with tidal asymmetry, play an important role in ETM formation and should be properly accounted for in studies on ETM dynamics in turbid estuaries.

Plain Language Summary In (highly) turbid estuaries, an estuarine turbidity maximum (ETM) with high suspended sediment concentrations (SSC) influences the water quality and the ecological system. These sediment suspensions interact with hydrodynamics, which in turn shapes the ETM, influencing the siltation of navigation channels, freshwater resources, and estuarine ecology. In this study, we developed a schematic model to investigate the role of sediment-induced density effects in combination with tidal asymmetry and water-bed exchange processes. Their combined effects affect the contribution of tidal pumping and estuarine circulation to landward sediment transport, leading to changes in ETM strength and location. These findings have implications for the management of sediment and freshwater resources in turbid estuaries.

1. Introduction

Many estuaries trap sediments in regions called the Estuarine Turbidity Maximum (ETM), resulting in locally elevated suspended sediment concentrations (SSC) (Schubel, 1968). ETM dynamics have been extensively studied through in-situ measurements (e.g., Fettweis et al., 1998; Jalón-Rojas et al., 2015, 2016; Mitchell et al., 2017) and numerical modeling (e.g., Brenon & Le Hir, 1999; Festa & Hansen, 1978; Geyer, 1993; Grasso et al., 2018; Kumar et al., 2017; Yu et al., 2014). ETMs are often associated with sediment trapping (e.g., Burchard et al., 2018) although they are not necessarily the same. ETMs are the result of converging sediment transport, where the seaward-directed transport in the upper estuary (predominantly driven by fluvial processes) is balanced by landward-directed transport components of marine origin. The most important landward transport components are (a) tidal asymmetry, commonly characterized by a stronger but shorter flood velocity and a weaker but longer ebb velocity (Brenon & Le Hir, 1999; Dyer, 1988; Friedrichs & Aubrey, 1988; Uncles et al., 1985; Yu et al., 2014) and (b) gravitational circulation, with longitudinal salinity gradients generating a landward residual flow close to the bed (Dyer, 1988; Festa & Hansen, 1978). Other mechanisms, for example, internal tidal asymmetry and tidal straining, strengthen sediment trapping as well (Jay & Musiak, 1994, 1996; Simpson et al., 1990).

The ETM location may greatly vary in space and time in different estuaries (Burchard et al., 2018). Spatially, ETMs may exist near the landward limit of the salt wedge, far into the freshwater zone, and within the estuarine salinity gradient (Burchard et al., 2018) and an estuary may even have multiple ETMs (Zhu, van Maren, et al., 2021). Temporally, the ETM location shows seasonal, spring-neap, and tidal variations (e.g., Grasso et al., 2018; Jalón-Rojas et al., 2015; Mitchell et al., 2017). It also varies over years due to human-induced forcing, for example, stronger flood dominance and reduced hydraulic drag due to deepening play an important role in the landward movement of ETM in the Ems estuary (Chernetsky et al., 2010). These variations of ETM location are closely related to the relative roles of major forcing driving sediment transport, which is more complex in combined river-and tide-dominated estuaries. For instance, the dominant up-estuary sediment transport mechanisms remain disputed in the upper Chesapeake Bay (Sanford et al., 2001; Schubel, 1968) and Yangtze Estuary (Li et al., 2018; Li & Zhang, 1998; Liu et al., 2011; Song et al., 2013).

Moreover, sediments, together with tidal asymmetry, influence the efficiency and location of sediment trapping. Numerical model results suggest that low settling velocities favor a downstream movement of the ETM (Brenon & Le Hir, 1999; Cheng et al., 2013; de Jonge et al., 2014; Dijkstra et al., 2019a; Yu et al., 2014). Asymmetries in sediment settling velocity and critical shear stress for erosion generate settling and scour lags (Friedrichs, 2011; Postma, 1961; van Straaten & Kuenen, 1957), which in combination with spatial or temporal hydrodynamic asymmetries contribute to estuarine sediment trapping (Chernetsky et al., 2010). Sediment-induced density effects (SedDE) may also play a role in ETM migration through horizontal sediment-induced density gradients (Talke et al., 2009; Zhu, van Maren, et al., 2021), vertical mixing (Lin et al., 2021; van Maren et al., 2020; Zhu, van Maren, et al., 2021) or modified bed roughness (Dijkstra et al., 2019b; Dijkstra, Schuttelaars, Schramkowski, Brouwer, 2019; Gabioux et al., 2005; Jalón-Rojas et al., 2018; van Maren et al., 2015; Zhu, Guo, et al., 2021). These sediment-induced density effects introduce a positive feedback between sediment trapping and tidal asymmetry: smoothening of the bed leads to tidal amplification in estuaries and therefore enhanced flood-dominated tidal flow (Gabioux et al., 2005; Jalón-Rojas et al., 2016, 2018; Wang et al., 2014; Zhu, Guo, et al., 2021), resulting in progressively more sediment trapping and potentially a regime shift toward hyper-turbid conditions (Dijkstra et al., 2019b; Dijkstra, Schuttelaars, Schramkowski, Brouwer, 2019; Lin et al., 2021; Winterwerp, 2011; Winterwerp & Wang, 2013; van Maren et al., 2015). Especially for relatively high SSC, the SedDE is essential for suppression of turbulence, promoting sediment settling (Winterwerp, 2001), and resulting in sediment trapping (van Maren et al., 2020; Winterwerp & van Kessel, 2003).

Recently, the strengthening effect of the near-bed sediment concentration on sediment trapping through the SedDE has been stressed (van Maren et al., 2020). The near-bed sediment concentration is influenced by water-bed exchange processes related to (a) the settling flux of sediment onto the bed by suppression of turbulence (increased settling velocity as elaborated above) and the settling velocity of particles, and (b) resuspension processes related to the critical shear stress for erosion of freshly deposited sediments. The near-bed sediment concentration is larger due to the reduced deposition flux and stronger resuspension processes in sediment-laden flows for the following reasons (see van Maren et al., 2020 for more details). The deposition flux is determined by the settling velocity and the sediment concentration. At high SSC, flocs break up in the highly sheared near-bed region, and therefore the settling velocity decreases close to the bed (Hill et al., 2001). Hindered settling leads to an overall reduction in the settling velocity and therefore less deposition at high SSC (Richardson & Zaki, 1954). In addition, consolidation scales quadratically with the thickness of the consolidating layer, and therefore the consolidation time increases with SSC (Gibson et al., 1967). Consequently, the critical shear stress for erosion is attained slowly and particles transported at high concentrations in a decelerating tidal flow are kept in suspension (close to the bed) for a longer time. On top of that, high near-bed SSC may also reduce the bed shear stress. These water-bed exchange processes lead to relatively high near-bed sediment concentrations, which influence hydrodynamics but also directly influence the relative role of residual flows (as in estuarine circulation) or resuspension processes (such as tidal pumping) on residual transport. However, these high near-bed SSC layers and the associated SedDE on ETM dynamics have not yet been explored in detail.

This study aims to understand ETM formation in terms of its location and growth due to the SedDE and high near-bed sediment concentrations for various types of tidal asymmetry in a systematic way. For this purpose, we developed a schematized model reflecting the hydrodynamics and sediment dynamics of the Yangtze Estuary, providing a well-studied example of an estuary where all the above-mentioned hydrodynamic and sedimentary processes play a role. Our goal here is not to provide a realistic simulation for this particular estuary, but rather

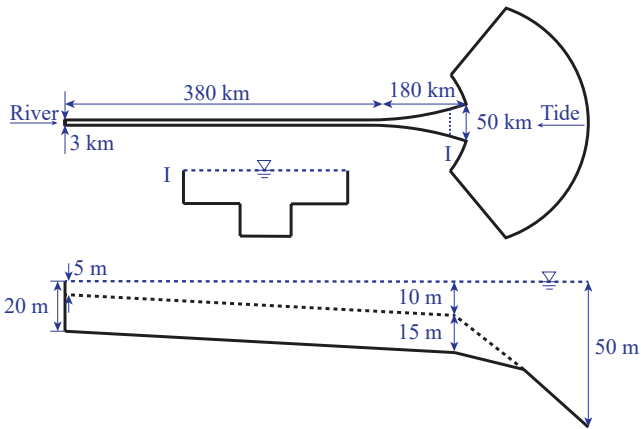


Figure 1. The planform and bathymetry of the schematic model. The x-axis is defined in the longitudinal seaward direction starting from the river boundary (km-0).

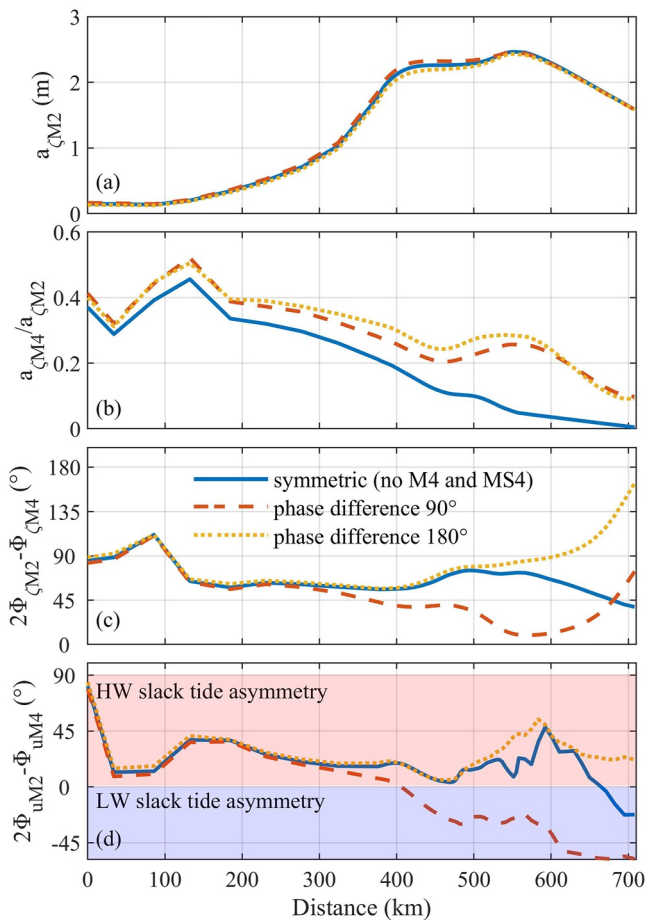


Figure 2. Tidal propagation in the scenarios with the symmetric tide (no M_4 and MS_4), asymmetric tides with phase differences of 90° and 180° , respectively: (a) Water level amplitude of M_2 ($a_{\zeta M2}$), (b) amplitude ratio of M_4 to M_2 ($a_{\zeta M4}/a_{\zeta M2}$), (c) phase difference between M_2 and M_4 for water levels ($2\phi_{\zeta M2} - \phi_{\zeta M4}$), and (d) phase difference between M_2 and M_4 for depth-averaged flow velocity ($2\phi_{u M2} - \phi_{u M4}$).

to gain insights into the roles of tidal asymmetries, sediment-induced density effects, and higher near-bed SSCs on ETM dynamics. The model setup, effects of sediments, and the methods for decomposing the net sediment transport flux are described in Section 2. Model results in terms of the effect of sediment settling velocity and critical bed shear stress, ETM formation, and sediment transport mechanisms are presented in Section 3. The effects of high sediment concentrations on ETM formation and sediment transport mechanisms are discussed in Section 4. Conclusions are drawn in Section 5.

2. Methods

2.1. Basic Model Setup

We construct a schematized three-dimensional (3D) estuarine model based on the open-source Delft3D code (Lesser et al., 2004). This modeling system simulates hydrodynamics and sediment transport and has been widely validated and used in varying estuarine and coastal environments. The generation, transport, and dissipation of turbulence are resolved with a k- ϵ model, in which turbulent mixing is modified by sediment-induced buoyancy effects through the equation of state.

The model has dimensions inspired by the Yangtze Estuary in which the origin of the axis is defined at the river boundary (km-0) (Figure 1). The width at km-560 represents multiple combined branches of the Yangtze Estuary except for the North Branch where a subtidal flow partition is $<5\%$ (Yun, 2004). It consists of a 560 km long basin with a width diverging from 3 km at the landward limit to 50 km at the mouth. The basin has a deep channel and shallow areas with a width that accounts for one-third and two-thirds of each cross-sectional width, respectively. The channel depth increases linearly from 20 m at the landward head (km-0) to 25 m at the mouth, after which the depth increases more rapidly to 50 m at the seaward boundary (710 km). The depth of the shallow areas increases linearly from 5 m at the origin to 10 m at the mouth. The banks of the estuary are non-erodible.

The model is forced with a simplified river discharge and tidal elevation. River discharge is prescribed with a constant value of $30,000 \text{ m}^3/\text{s}$, which is the approximate annual mean river discharge of the Yangtze River. Tidal water level constituents (M_2 , S_2 , M_4 , and MS_4) are prescribed at the seaward boundary (amplitudes of 1.5, 1, 0.15, and 0.15 m, respectively) with different water level phase relations to explore the effect of tidal asymmetry: (a) Symmetric tides (no M_4 and MS_4 component); (b) asymmetric tides with water level phase differences of 90° (with $2\phi_{\zeta M2} - \phi_{\zeta M4} = 90^\circ$ and $2\phi_{\zeta S2} - \phi_{\zeta MS4} = 90^\circ$); (c) asymmetric tides with water level phase differences of 180° (with $2\phi_{\zeta M2} - \phi_{\zeta M4} = 180^\circ$, $2\phi_{\zeta S2} - \phi_{\zeta MS4} = 180^\circ$). Note that the type of tidal asymmetry varies throughout the estuary due to tidal deformation (Figure 2). The type of tidal asymmetry is determined by the phase lag in the velocity of M_2 and M_4 components ($\theta_u = 2\phi_{u M2} - \phi_{u M4}$). For $\theta_u = -90^\circ \sim 90^\circ$, the peak flood flow velocity is larger than the peak ebb flow velocity (with maximum flood-dominance at $\theta_u = 0^\circ$), see Friedrichs & Aubrey, 1988), which leads to landward transport due to peak flood tidal dominance. For $\theta_u = 0^\circ \sim 180^\circ$ (maximal flood-dominance at $\theta_u = 90^\circ$), the duration of high water (HW) slack is longer than that of low water (LW) slack, leading to landward sediment transport due to HW slack tide dominance. Sediment transported landward during flood therefore has a longer period to settle at HW slack tide than at LW slack tide, resulting in net landward transport (Dronkers, 1986). The computed velocity phase difference θ_u

for offshore water level phase differences of 90° is approximately -30° at km-560, and therefore the tide at the mouth is mainly flood dominant due to peak flow asymmetry but slightly ebb dominant due to LW slack tide asymmetry. Similarly, for an offshore water level phase difference of 180° , $\theta_u = 45^\circ$ at the mouth and therefore the tide is flood dominant because of peak flow asymmetry and HW slack tide asymmetry.

The sediment dynamics are computed using the Partheniades equation (Partheniades, 1965) for erosion E , and a permanent deposition flux D (Sanford & Halka, 1993):

$$E = M \left(\frac{\tau}{\tau_{cr}} - 1 \right) \quad (1)$$

$$D = \alpha \omega_s c \quad (2)$$

where M is the erosion rate ($\text{kg/m}^2/\text{s}$), τ is the bed shear stress, τ_{cr} the critical bed shear stress for erosion, ω_s the settling velocity (m/s), c the SSC (kg/m^3), and α is a reduced deposition factor introduced by van Kessel and Vanlede (2010) to approximate complex and poorly understood water-bed exchange processes which are not explicitly modeled (see more details hereafter). The settling velocity is composed of a clear water settling velocity ω_{s0} , which is reduced by hindered settling effects using a simple power law equation based on Richardson and Zaki (1954):

$$\omega_s = \omega_{s0} (1 - c/c_{ref})^5 \quad (3)$$

where c_{ref} is the gelling concentration when a space-filling network of sediment particles develops at or above which the suspension starts to behave more like a solid. In the Yangtze Estuary, the near-bed SSC varies from several 1's to 10's of kg/m^3 as concentrated benthic suspensions and from several tens to a few hundred as fluid mud (Lin et al., 2019, 2021; Wan, Roelvink, et al., 2014). Here, we prescribe the gelling concentration as 200 kg/m^3 which is larger than its typical value for clay-dominated suspensions ($30\text{--}180 \text{ kg/m}^3$) because of the relatively high silt content (van Maren, Winterwerp, Wang et al., 2009; van Maren, Winterwerp, Wu et al., 2009).

Finally, the model is initialized without sediment on the bed and with no morphological changes. All sediment enters the domain through the upstream river boundary (a constant SSC of 0.2 kg/m^3 , approximately the yearly mean SSC at the river boundary of the Yangtze Estuary), and the model is run until the computed SSC reaches dynamic equilibrium (i.e., a condition where the SSC only varies over the tidal and spring-neap tidal cycles but no longer displays a trend). For more details on model setup, parameter settlings, and behavior, we refer to the Supporting Information S1.

2.2. Effects of Sediments

Sediments influence the hydrodynamics by damping of turbulence (computed with a k- ϵ model) and through horizontal density gradients driving longitudinal and lateral flows. Both result from the contribution of sediment to the water density which is computed as:

$$\rho = \rho_w + \left(1 - \frac{\rho_w}{\rho_s} \right) c \quad (4)$$

where ρ_w is the clear sea-water density (see SM), and ρ_s is the sediment density ($2,650 \text{ kg/m}^3$). The effect of sediment on density is evaluated by comparing model simulations with (scenario “Full”) and without (scenario “Sal”) the sediment density coupling.

The sediment concentration itself also introduces several feedback mechanisms related to the settling and erosion of sediments, influencing the exchange of sediments between the water column and bed. At high sediment concentrations with sufficiently strong sediment trapping, water-bed exchange processes (Section 1, see also van Maren et al., 2020 for details) lead to higher near-bed SSC at high sediment concentrations. However, they are either not sufficiently understood from a physical point of view (floc destruction in the near-bed boundary layer, strength development of soils at short time scales) or cannot be represented in large-scale numerical models from a computational point of view (a sufficiently high vertical resolution to account for the hindered settling effects,

floc destruction in the near-bed boundary layer). The combined effect of these processes is parameterized by the reduced deposition factor α introduced earlier (van Kessel & Vanlede, 2010; van Maren et al., 2020).

With the current state of knowledge, it is not clear which water-bed exchange process is more important. However, their combined effect is a reduced sediment flux into the bed and/or increased resuspension. This leads to higher near-bed sediment concentrations which are more pronounced in high SSC environments, for example, ETMs. The combined effect of these water-bed exchange processes is evaluated through scenarios in which the deposition efficiency is varied (using $\alpha = 1, 0.5, 0.3,$ and 0.1 representing conditions without reduced deposition to strongly reduced deposition).

2.3. Net Sediment Transport

To explore the relative importance of various mechanisms contributing to residual sediment transport, the net sediment transport flux per unit width over a spring-neap tidal cycle F (kg/m/s) can be decomposed as follows (Dyer, 1988, 1997):

$$F = \frac{1}{T} \int_0^T \int_0^1 hucdzdt$$

$$= \underbrace{h_0 \overline{u_0 c_0}}_{F1} + \underbrace{\overline{c_0} \langle h_t \overline{u_t} \rangle}_{F2} + \underbrace{\overline{u_0} \langle h_t \overline{c_t} \rangle}_{F3} + \underbrace{h_0 \langle \overline{u_t} \overline{c_t} \rangle}_{F4} + \underbrace{\langle h_t \overline{u_t} \overline{c_t} \rangle}_{F5} + \underbrace{h_0 \overline{u'_0 c'_0}}_{F6} + \underbrace{h_0 \langle \overline{u'_t c'_t} \rangle}_{F7} \quad (5)$$

where h is the water depth; z is relative depth, $0 \leq z \leq 1$; c is the SSC, u is the current velocity, and T is the spring-neap tidal period. The subscript 0 means tidally averaged, the subscript t denotes tidally fluctuating and the quotation marks denote a depth-dependent term. Angled brackets ($\langle \rangle$) and overbars ($\overline{}$) signify the means over the tidal cycles and the depth, respectively. Each decomposed term represents a particular mechanism contributing to sediment transport. The first term (F1) is the non-tidal drift known as the Eulerian flux whereas the second term (F2) is the flux induced by the Stokes' drift. The two terms (F1 + F2) combined provide the advective sediment flux (the Lagrangian flux, F_a). Terms F3, F4, and F5 are generated by the tidal phase differences between the depth-averaged SSC, the depth-averaged velocity, and the tidal elevation. Term F6 represents the tidally averaged vertical circulation, which can be interpreted as estuarine circulation (F_e); Term F7 arises from the non-uniform vertical distribution of velocity and SSC. Typically, terms F3, F4, and F5 are tidal pumping terms (Dyer, 1988) although term F7 is also regarded as tidal pumping in some studies (Burchard et al., 2018; Dijkstra et al., 2019b). Burchard et al. (2018) described tidal pumping as tidal covariance transport due to the correlation between SSC and current velocities, for example, up-estuarine transport due to higher depth-mean SSC during flood than during ebb. Term F7 represents the combined vertical and temporal covariance transport which may result from internal asymmetries in mixing and settling velocity (Burchard et al., 2018). In this study, we adopt the tidal pumping terms (F_t) as the sum of the terms F3, F4, F5, and F7. We also compute the decomposed longitudinally averaged sediment transport flux per unit width F_L (kg/m/s) in the thalweg of the deep channel between 380 and 560 km, including the transport by advection ($F_{a,L}$), tidal pumping ($F_{t,L}$), and estuarine circulation ($F_{e,L}$). This decomposition method has been widely applied to the study of sediment flux patterns in estuaries (e.g., Li et al., 2018; Li & Zhang, 1998; Liu et al., 2011; Uncles et al., 1985; Uncles & Stephens, 1993). Analysis of the decomposed terms reveals the relative importance of different transport processes, which is important for understanding the formation mechanisms of ETMs.

3. Results

3.1. Sensitivity to Sediment Properties

We evaluate the effects of the sediment settling velocity and critical bed shear stress for erosion for three types of tidal asymmetry, and for various sediment-induced density effects (Figure 3). For all types of tidal asymmetry, the strongest sediment trapping occurred with the smallest critical bed shear stress ($\tau_{cr} = 0.1$ Pa). However, the impact of tidal asymmetry was more complex for the sediment settling velocity. Settling velocities of 0.5 mm/s, 2 mm/s, and 0.5 mm/s lead to the strongest sediment trapping (respectively) for the symmetric tides and asymmetric tides with phase differences of 90° and 180°. The model with tidal phase differences of 180° shows the most pronounced influence of the sediment settling velocity on sediment trapping.

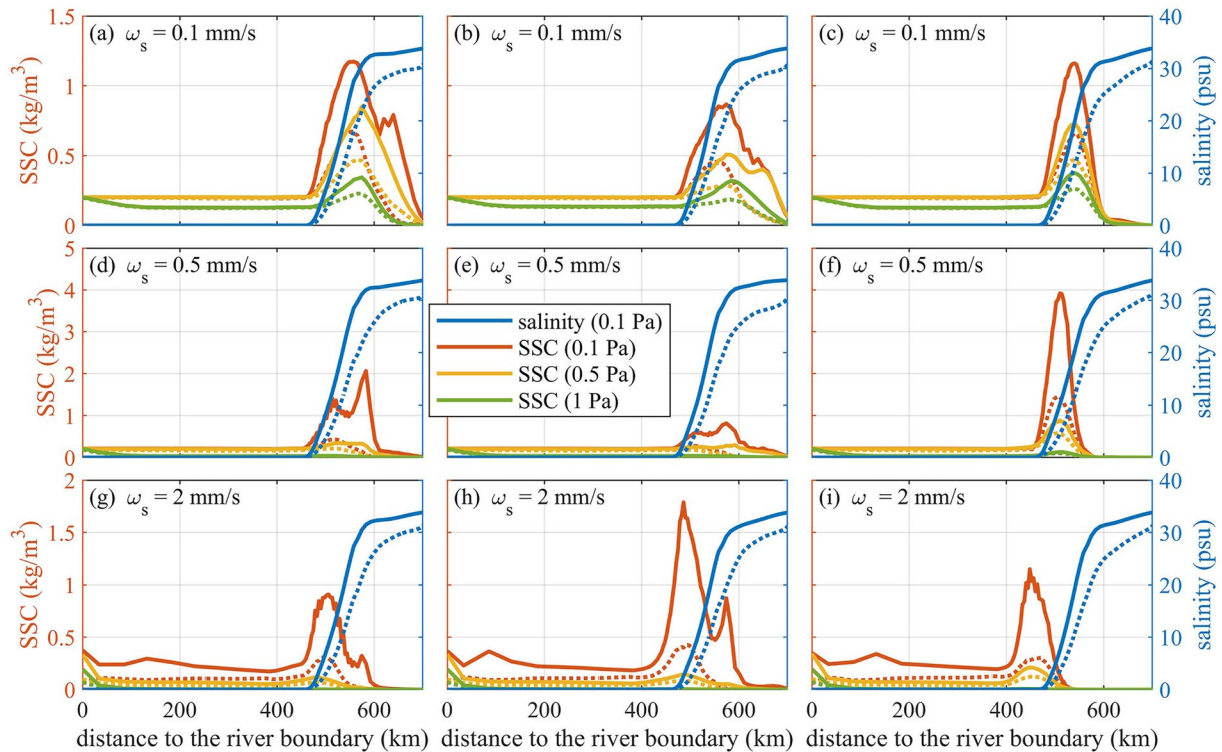


Figure 3. Modeled longitudinal distribution of averaged bottom (solid line) and surface (dotted line) suspended sediment concentration (SSC) and salinity (blue, only τ_{cr} of 0.1 Pa is shown) in the thalweg over a spring-neap tidal cycle with settling velocity ω_s of (a–c) 0.1 mm/s; (d–f) 0.5 mm/s; (g–i) 2 mm/s and bed sediment with critical shear stress for erosion τ_{cr} of 0.1 Pa (red), 0.5 Pa (yellow) and 1 Pa (green). The models are prescribed with (a, d and g) symmetric tides, asymmetric tides with phase differences of (b, e and h) 90° and (c, f and i) 180° with sediment-induced density gradient.

For all types of tidal asymmetry, the location of the maximum SSC of the ETM strongly depends on the sediment settling velocity, particularly for tidal asymmetry with phase differences of 180° . Sediment with a large settling velocity (2 mm/s) is more efficiently transported up-estuary just landward of the tip of the salt wedge, whereas the ETM remains further seaward for sediment with a smaller settling velocity (0.5 mm/s and 0.1 mm/s). The critical bed shear stress slightly influences the location of the maximum SSC of the ETM for the smallest settling velocity of 0.1 mm/s. Tidal asymmetry leads to landward movement of the location, which is most pronounced when the settling velocity is 2 mm/s.

The ETM of the Yangtze Estuary is located at the tip of the salt wedge (as for $\omega_s = 2$ mm/s) with a peak SSC of several kg/m^3 (as for $\tau_{cr} = 0.1$ Pa) for river discharges in both dry and wet seasons varying from 10,000 to 50,000 m^3/s (e.g., Lin et al., 2019; Liu et al., 2011; Wan, Gu, et al., 2014). To reproduce the basic ETM dynamics in the Yangtze Estuary, we will therefore prescribe sediment with $\tau_{cr} = 0.1$ Pa and $\omega_s = 2$ mm/s for further analysis of sediment-induced density effects and tidal asymmetry.

3.2. ETM Formation

The ETM location and growth is not only influenced by tidal asymmetry and sediment properties (as in Figure 3) but also by complex transport processes operating close to the bed (parameterized with reduced deposition α , as explained in Section 2.2). The sediment concentrations in Figure 3 are SSC levels averaged over a spring-neap tidal cycle, computed without initial sediment on the bed but only by erosion and settling parameters and the open boundary sediment influx. SSC trapping is a delicate balance between settling and resuspension, with the equilibrium SSC depending on sediment properties (settling, erosion). Higher SSC levels (resulting from the sediment properties) in turn impact hydrodynamics and therefore overall sediment dynamics.

Reduced deposition and sediment-induced density effects (SedDE) both lead to a pronounced increase in SSC, especially in combination with tidal asymmetry (both types of asymmetry, see Figure 4). Without SedDE and

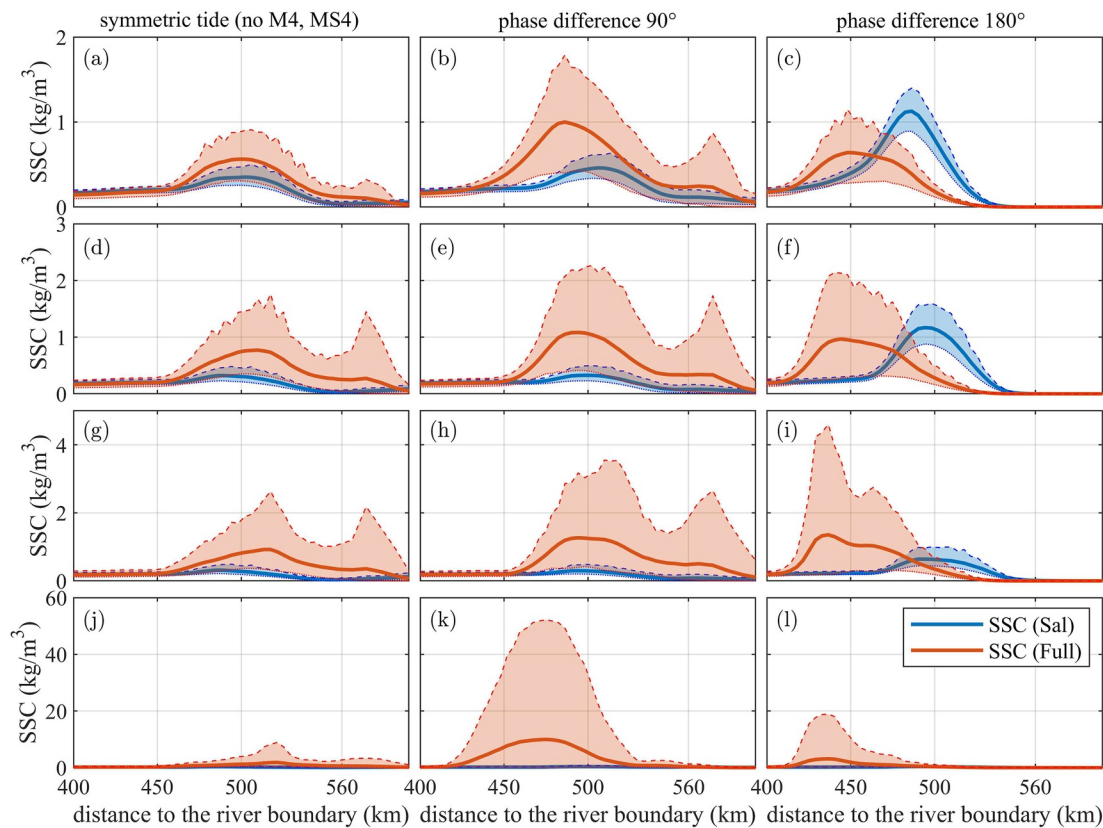


Figure 4. Comparison between the modeled longitudinal distribution of depth-averaged (solid line), surface (lower bounded dotted line) and bottom (up bounded dashed line) suspended sediment concentration (SSC) with (Full, in red) and without (Sal, in blue) sediment-induced density effect (SedDE) averaged over a spring-neap tidal cycle. Left, middle and right panels refer to scenarios with the symmetric tides (no M_4 and MS_4), asymmetric tides with water level phase differences of 90° and 180° , respectively. Top to bottom panels are scenarios with reduced deposition factor of (a–c) 1, (d–f) 0.5, (g–i) 0.3, and (j–l) 0.1. Note that the x-axis scales differ from those in Figure 3.

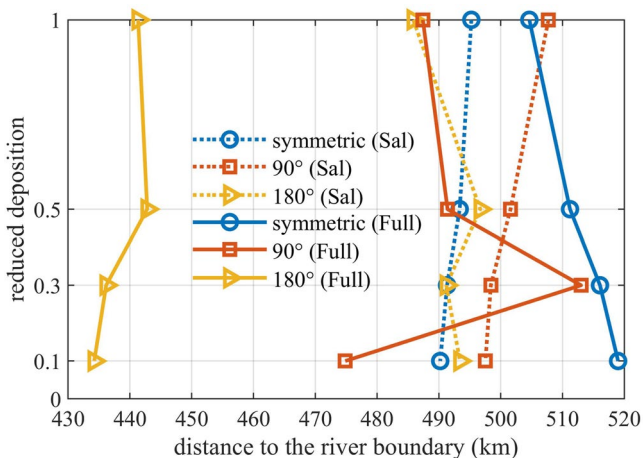


Figure 5. Modeled spring-neap averaged estuarine turbidity maximum (ETM) location (see Figure 4) influenced by the reduced deposition with the symmetric tides (no M_4 and MS_4) and asymmetric tides with phase differences of 90° and 180° , and with (Full, solid line)/without (Sal, dashed line) sediment-induced density effect (SedDE).

a reduction of water-bed exchange, a stronger flood dominance leads to progressively more sediment trapping (most pronounced for asymmetric tides with a phase difference of 180° : flood dominance due to peak flow asymmetry and HW slack tide asymmetry) (Figures 4a–4c). Sediment trapping is further enhanced with SedDE, except for asymmetric tides with phase differences of 180° (Figure 4c). This suggests that the SedDE in combination with tidal asymmetry, is important for trapping sediment. A reduction in water-bed exchange leads to a higher near-bed SSC (for all cases), which enhances stratification (see MS) and in turn influences the sediment trapping efficiency. Particularly for asymmetric tides with phase differences of 90° , the SSC may increase by a factor of 10 when the deposition flux is reduced by a factor of 10 as well (Figure 4k). We will elaborate on the relevance of these findings in more detail in the discussion.

The location of the ETM is therefore not only determined by the type of tidal asymmetry, but also by the high near-bed SSC resulting from reduced deposition and the SedDE (Figure 5). Here we define the spring-neap averaged ETM location as the mean position within the channel thalweg where the SSC exceeds the 90th percentile of the averaged near-bed SSC. For symmetric tides without the SedDE, reduced deposition leads to landward movement of the ETM. However, accounting for the SedDE, the ETM moves 10 km seaward without reduced deposition ($\alpha = 1$) and another 14 km seaward with

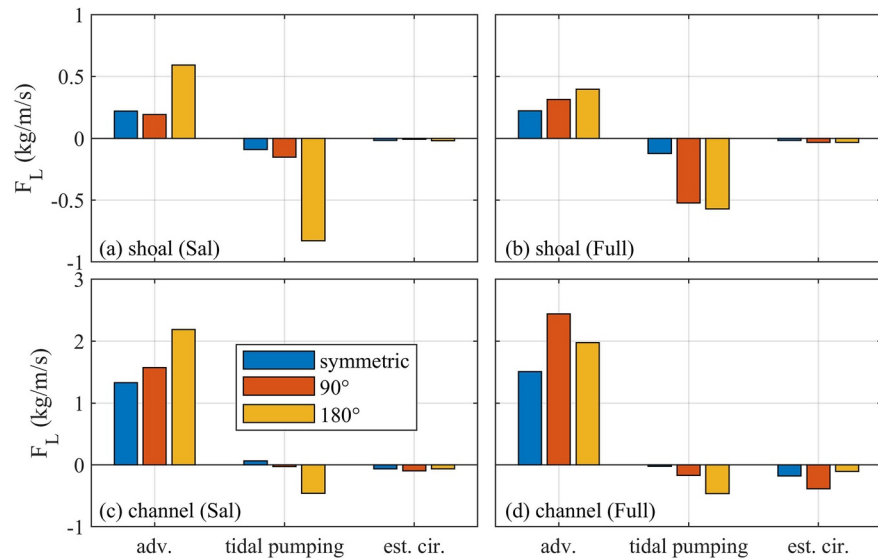


Figure 6. Decomposed longitudinally averaged sediment transport flux per unit width F_L (kg/m/s) in scenarios without reduced deposition ($\alpha = 1$) on the shallow shoals (a and b) and in the thalweg of the deep channel (c and d) without (Sal: a and c) and with (Full: b and d) the sediment-induced density effect (SedDE) induced by advective transport ($F_{a,L}$), tidal pumping ($F_{t,L}$), and estuarine circulation ($F_{e,L}$). Positive values indicate the ebb direction and negative values indicate the flood direction.

the strongest reduced deposition ($\alpha = 0.1$). For asymmetric tides, both landward and seaward migration of the ETM could occur without the SedDE due to stronger reduced deposition. With the SedDE and no reduced deposition ($\alpha = 1$), the ETM significantly moves landward by 20 and 45 km for asymmetric tides with phase differences of 90° and 180°, respectively. Although seaward migration of the ETM may occur with reduced deposition of 0.3 and 0.5 with the SedDE, the strongest reduced deposition of 0.1 also enhances landward migration by 13 and 7 km compared to that without reduced deposition for asymmetric tides with phase differences of 90° and 180°, respectively.

3.3. Decomposition of Sediment Transport Terms

To explain the computed ETM dynamics in the main channel and shallow areas, the residual sediment transport is decomposed into the contributions of advection, tidal pumping, and estuarine circulation (Figure 6, following the procedure described in Section 2.3). Note that even though the simulations are in dynamic equilibrium, residual sediment transport may exist due to sediment supply from the landward boundary and net sinks within the estuary (see SM). We first focus on the effect of tidal asymmetry and the SedDE on these transport terms, followed by an analysis of the contribution of reduced deposition.

In shallow areas, landward sediment transport is mainly caused by tidal pumping rather than estuarine circulation (Figures 6a and 6b). In addition, both with and without the SedDE, seaward advective transport overcomes landward sediment transport by tidal pumping for symmetric tides. For asymmetric tides with phase differences of 90°, the seaward advective transport is relatively larger than the landward sediment transport by tidal pumping without the SedDE, whereas tidal pumping is larger than advective transport. For asymmetric tides with a phase difference of 180°, landward sediment transport due to tidal pumping is larger than seaward advective transport without the SedDE, while with the SedDE, the contributions of both tidal pumping and advection are reduced. Although tidal pumping plays an important role in the channel and over the shoal, the advective sediment flux is much larger in the channel than shoal. Therefore, unless explicitly mentioned otherwise, in the following section we elaborate on the effects of tidal asymmetry, SedDE, and reduced deposition in the deep channel.

In the channel, both tidal pumping and estuarine circulation play an important role in landward sediment transport (Figures 6c and 6d). Without the SedDE, the contribution of the tidal pumping term varies with the type of tidal asymmetry: symmetric tides lead to seaward sediment transport but asymmetric tides with phase differences

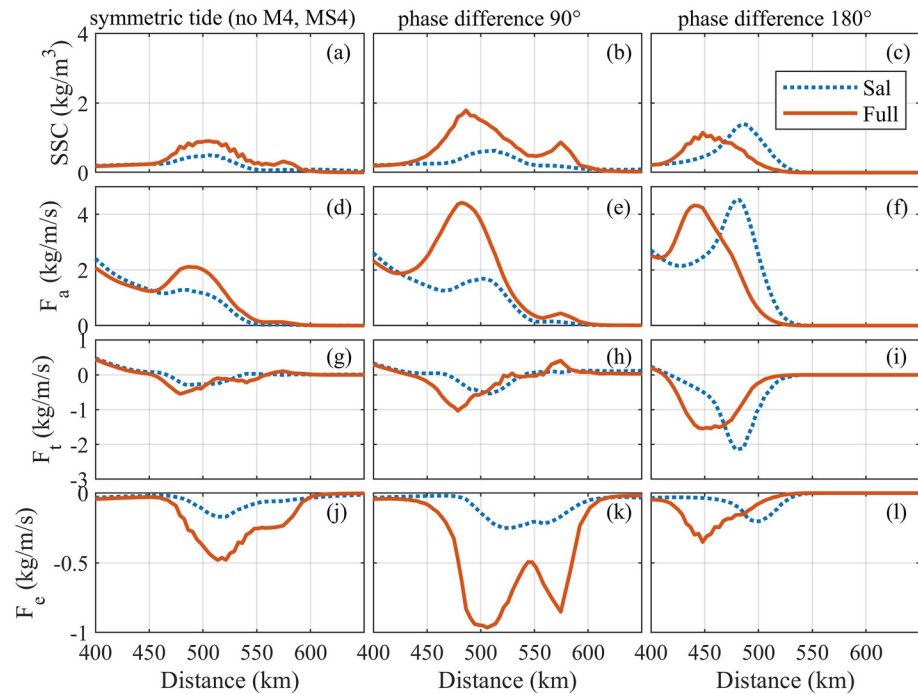


Figure 7. Modeled longitudinal distribution of (a, b and c) near-bed suspended sediment concentration (SSC) and decomposed sediment flux per unit width F (kg/m/s) for cases with (Full, solid red line) and without (Sal, blue dotted blue line) sediment-induced density effect (SedDE) with no reduced deposition ($\alpha = 1$). The residual sediment flux is decomposed into (d, e and f) advective transport F_a , (g, h and i) tidal pumping F_t , and (j–l) estuarine circulation in the deep channel F_e . Left, middle and right panels refer to scenarios with the symmetric tides (no M_4 and MS_4), asymmetric tides with water level phase differences of 90° and 180° , respectively. Positive values indicate the ebb direction and negative values indicate the flood direction. The sum of the different transport terms deviates from 0 because of the lateral variation of residual transport.

of 90° and 180° lead to landward sediment transport, especially for asymmetric tides with phase differences of 180° . The effects of estuarine circulation are similar for all types of tidal asymmetry. With the SedDE, both tidal pumping and estuarine circulation are enhanced for symmetric tides and asymmetric tides with phase differences of 90° whereas estuarine circulation is mainly strengthened for asymmetric tides with phase differences of 180° . Therefore, the largest impact of adding sediment-induced effects in the channel is the much stronger landward sediment transport due to tidal pumping and estuarine circulation, with their relative contributions depending on the tidal asymmetry.

In this study, we further elaborate on density effects through their interaction with tidal asymmetry (Figure 7). With salinity-induced density gradients only (Sal scenario), an ETM is formed at around km-500 for all types of tidal asymmetry (Figures 7a–7c). Tidal asymmetry with stronger flood dominance shows larger sediment trapping, corresponding to the stronger seaward advective transport and landward sediment transport by tidal pumping (Figures 7d–7i). Note that tidal pumping may also lead to seaward sediment transport when flood dominance is weak (for asymmetric simulations, see Figure 6c). Estuarine circulation is slightly stronger for asymmetric tides with phase differences of 90° than for symmetric tides and for asymmetric tides with phase differences of 180° (Figures 7j–7l).

The combined effect of salinity- and sediment-induced density effects (Full scenario) leads to 50% higher SSC for symmetric tides and asymmetric tides with phase differences of 90° but slightly lower SSC for asymmetric tides with phase differences of 180° (Figures 7a–7c). The changes in the magnitude of the maximum SSC of the ETM are consistent with the changes in the contribution of advection and tidal pumping. Specifically, advection and tidal pumping are enhanced for symmetric tide and asymmetric tides with phase differences of 90° , but weakened for asymmetric tides with phase differences of 180° (Figures 7d–7i). Estuarine circulation is enhanced for all types of tidal asymmetry, particularly for asymmetric tides with phase differences of 90° (Figures 7j–7l). In addition, tidal asymmetry with stronger flood dominance leads to more pronounced landward migration of the ETM

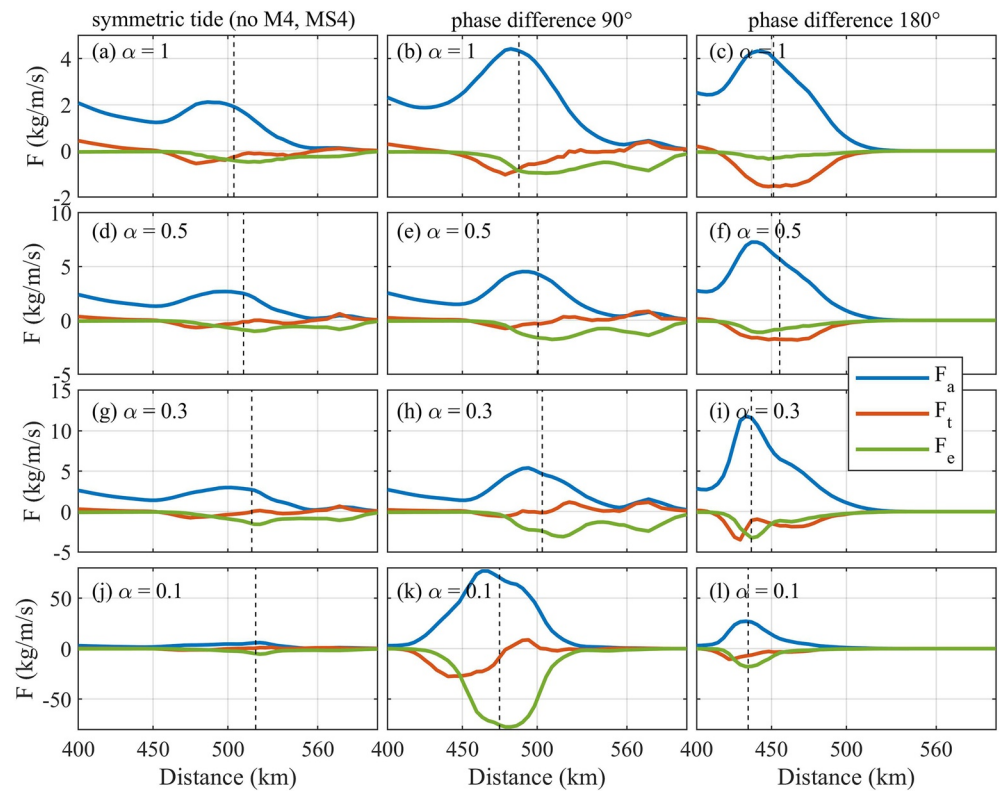


Figure 8. Decomposed sediment transport flux per unit width F (kg/m/s) in scenarios with the sediment-induced density effect (SedDE) induced by advective transport (F_a), tidal pumping (F_t), and estuarine circulation (F_e) in scenarios for sediment settling velocity of 2 m/s and critical bed shear stress of 0.1 Pa. Left, middle and right panels refer to scenarios with the symmetric tides (no M_4 and MS_4), asymmetric tides with water level phase differences of 90° and 180° , respectively. Top to bottom panels are scenarios with reduced deposition α of 1, 0.5, 0.3, and 0.1, respectively. The vertical dashed lines indicate the location of the estuarine turbidity maximum (ETM) (see Figure 4). Positive values indicate the ebb direction and negative values indicate the flood direction. The relative contributions of the mechanisms in panel j are not visible to keep scaling consistent with panels k and l, but the longitudinal patterns are comparable with panels k and l. The sum of the different transport terms deviates from 0 because of the lateral variation of residual transport.

(Figures 7a–7c), corresponding to the enhanced landward movement resulting from advection, tidal pumping, and estuarine circulation (Figures 7d–7l).

As a next step, we evaluate the impact of reduced deposition on advection, tidal pumping, and estuarine circulation. Stronger reduced deposition with higher near-bed SSC influences the relative importance of advection, tidal pumping, and estuarine circulation (Figures 8 and 9). Stronger reduced deposition results in a shift of the location of the maximum sediment transport contribution, depending on tidal asymmetry and corresponding to the ETM migration (see Figure 5). Specifically, for the symmetric tide, the maximum sediment transport contributed by estuarine circulation migrates seaward due to stronger reduced deposition. The maximum sediment transport driven by tidal pumping and estuarine circulation migrates landward for asymmetric tides with strongest reduced deposition ($\alpha = 0.1$) compared to weaker reduced deposition ($\alpha = 0.3, 0.5$, and 1). In addition, the contribution of tidal pumping to up-estuary transport is comparable to (for symmetric tides and asymmetric tides with phase differences of 90°) or exceeds (for asymmetric tides with phase differences of 180°) that of estuarine circulation without reduced deposition ($\alpha = 1$) (Figures 8a–8c). With stronger reduced deposition, the effect of estuarine circulation becomes progressively larger (for all types of tidal asymmetry). On the other hand, tidal pumping may result in longitudinal spreading of the concentration peaks in the ETM, both for symmetric tides and asymmetric tides with phase differences of 90° (evident as a transport flux changing direction in the along-estuary direction, see Figure 8).

The longitudinally averaged sediment transport fluxes in the deep channel (F_L) are also evaluated (Figure 9). For all simulations, symmetric tides and asymmetric tides with phase differences of 90° lead to a relatively

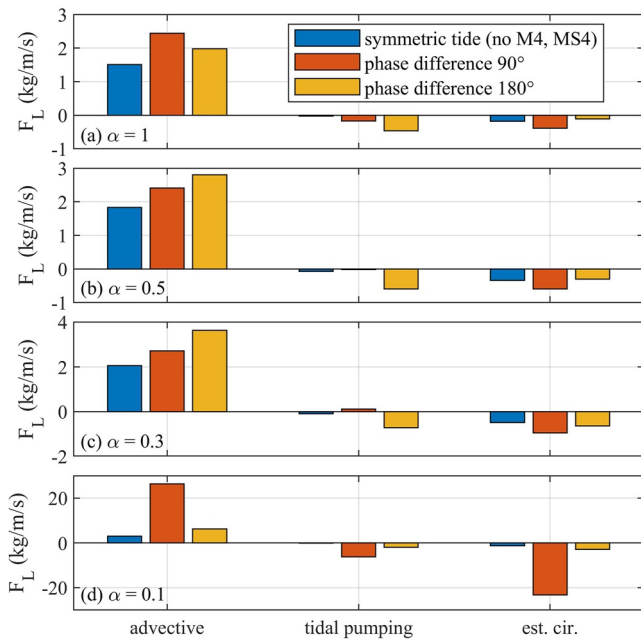


Figure 9. Decomposed longitudinally averaged sediment transport flux per unit width F_L (kg/m/s) in scenarios with the sediment-induced density effect (SedDE) induced by advective transport ($F_{a,L}$), tidal pumping ($F_{t,L}$), and estuarine circulation ($F_{e,L}$) in scenarios for sediment settling velocity of 2 m/s and critical bed shear stress of 0.1 Pa. Top to bottom panels are scenarios with reduced deposition (a) $\alpha = 1$; (b) $\alpha = 0.5$; (c) $\alpha = 0.3$ and (d) $\alpha = 0.1$, respectively. Positive values indicate the ebb direction and negative values indicate the flood direction. The sum of the different transport terms deviates from 0 because of the lateral variation of residual transport.

smaller contribution of tidal pumping to up-estuary sediment transport than estuarine circulation. This is probably caused by the longitudinal spreading near the concentration peaks in the ETM as stated above. Similarly, due to this effect, tidal pumping may be weakened with larger reduced deposition for symmetric tides and asymmetric tides with phase differences of 90° . For asymmetric tides with phase differences of 180° , the contribution of estuarine circulation is smaller than that of tidal pumping without reduced deposition ($\alpha = 1$). Stronger reduced deposition increases the contribution of estuarine circulation which outweighs the contribution of tidal pumping with the strongest reduced deposition ($\alpha = 0.1$).

4. Discussion

4.1. Effect of High Concentrations on ETM Formation

ETM migration and growth is strongly related to the SedDE, tidal asymmetry, and reduced deposition. Typically, stronger flood dominance imports more sediment and leads to further landward migration of the ETM. Vertical SSC gradients suppress turbulence, increase vertical and longitudinal salinity-induced density gradients and gravitational circulation, which further increases vertical SSC gradients and provides a positive feedback for trapping sediment (Dijkstra et al., 2019b; Winterwerp et al., 2009; Zhu, van Maren, et al., 2021). Reduced deposition parameterizes the effect of poorly understood near-bed processes such as consolidation, flocculation, and hindered settling on the vertical sediment concentration gradient (van Maren et al., 2020; Winterwerp et al., 2021). The SedDE accounts for the impact of turbulence suppression by sediment-induced density gradients higher up in the water column on vertical concentration gradients, which is a much better understood and quantified mechanism (Winterwerp, 2001). Despite the relatively weak theoretical foundation of reduced deposition, its effect (near bed SSC of several tens of kg/m^3) is a realistic phenomenon and essential for modeling sediment dynamics in systems such as the Yangtze Estuary.

For symmetric tides, the internally generated tidal asymmetry at the mouth (560 km) is flood dominant ($\theta_u = 20^\circ$) but weaker than for asymmetric tides (see Figure 2) and therefore not able to trap and transport sediment landward. Moreover, our model results suggest a higher near-bed SSC for asymmetric tides with phase differences of 180° than for 90° without the SedDE (Figures 4 and 7). With the SedDE, sediment trapping is weaker for asymmetric tides with phase differences of 180° than without, which is probably caused by the effects of longitudinal SSC gradients on decreasing the magnitude of the SSC in the ETM (Zhu, vanMaren, et al., 2021). However, stronger reduced deposition leads to stronger sediment trapping with the SedDE for all types of tidal asymmetry, including asymmetric tides with phase differences of 180° .

Whether slack tide asymmetry or peak flow asymmetry contributes more to transport also depends on the type of transported sediment. Rapidly settling sediment with a large critical shear stress for erosion (sand), especially when available in great quantities, is very susceptible to peak flow asymmetry (Friedrichs, 2011). We prescribe sediments with a low critical shear stress for erosion, and with $\omega_s = 2$ mm/s (typically for a grain size of 50 μm , corresponding to 7.2 m/hr) in our Yangtze prototype. This means that for a short slack tidal period (~ 0.5 hr), only a small amount of sediment settles, whereas the majority of sediment settles for a long slack tidal period (~ 1.5 hr). The conditions in the deep channel therefore favor a pronounced landward sediment transport for the asymmetric tides with phase differences of 180° (minor HW slack tide dominance). Moreover, asymmetric tides with phase differences of 90° (limitedly LW slack tide dominant) in combination with the SedDE may lead to seaward sediment transport due to higher near-bed sediment concentrations despite peak flood tidal dominance (Figures 4 and 5). Therefore, although residual sediment transport is driven by many subtle processes, we believe that for easily erodible sediment, the large difference in the available time for particles to settle during slack tide, as a result of slack tide asymmetry, is the key mechanism driving maximum residual transport.

4.2. Effect of High Concentrations on Sediment Transport

ETMs are the result of various trapping mechanisms working simultaneously, as introduced earlier. We evaluated the contributions of tidal pumping and estuarine circulation to up-estuary sediment transport and observed that the SedDE, in combination with tidal asymmetry and reduced deposition, is important for understanding their relative roles (especially with estuarine circulation becoming more important at stronger SedDE).

Tidal pumping, primarily driven by tidal asymmetry, may be strengthened or weakened by the SedDE for asymmetric tides with phase differences of 90° and 180° , respectively, correspondingly leading to higher and lower near-bed SSC. This effect is especially important when tidal pumping dominates landward sediment transport with no or weak reduced deposition (Figure 4). Stronger reduced deposition leads to a progressively larger contribution of a landward transport component driven by estuarine circulation (Figures 8 and 9). The large contribution of estuarine circulation is the result of high near-bed concentrations, which are (a) most sensitive to the landward current near the bed generated by the longitudinal salinity gradients (Dyer, 1988; Festa & Hansen, 1978) but (b) also strengthen salinity-driven flows. This positive feedback between sediment and salinity was identified by Zhu, vanMaren, et al. (2021): The SedDE enhances along-channel salinity-induced density gradients and stratification, strengthening estuarine circulation.

4.3. Implications for ETM Dynamics: A Synthesis

Despite its geometric simplicity, our model provides a useful instrument to analyze ETM formation processes in response to tidal asymmetries in combination with sediment-induced effects (related to turbulent mixing, horizontal density gradients, and near-bed effects). Our results are partly generic and partly site-specific. Our site-specific results contribute to the understanding of the Yangtze Estuary. For instance, the water level phase difference $2\phi_{\zeta M2} - \phi_{\zeta M4}$ at the mouth of the Yangtze is $\sim 80^\circ$ (Guo et al., 2015; Lu et al., 2015; Zhu, Guo, et al., 2021). Our results suggest that for such an asymmetry, sediment-induced effects lead to an increasing SSC within the ETM rather than an upstream migration of the ETM (Figure 4). This may be the reason that siltation rates in the Yangtze Estuary navigation channel are so strong and the ETM remains stationary (Jiang et al., 2013; Liu et al., 2011). Our results also suggest that a change in sediment supply to the Yangtze Estuary (due to, e.g., a reduction in upstream sediment supply) may have a stronger impact than just a lowering of SSC in the ETM. The established relationships between sediment effects, tidal pumping, and estuarine circulation could also hold for other estuaries. For instance, in the Ems estuary, the ETM was observed to migrate in a landward direction into the freshwater zone (Talke et al., 2009). At the mouth of the upper Ems estuary, the water level phase difference $2\phi_{\zeta M2} - \phi_{\zeta M4}$ is $\sim 170^\circ$ (Chernetsky et al., 2010; van Maren et al., 2015), corresponding to the dominance of HW slack tide asymmetry. Figures 4 and 5 suggest that sediment-induced effects under such conditions lead to a landward migration of the ETM (even though the influence of salinity-driven flow is much weaker in the Ems than in the Yangtze Estuary). Within the ETM of the Ems estuary, $2\phi_{\zeta M2} - \phi_{\zeta M4}$ becomes $\sim 90^\circ$ for which our results suggest sediment-induced effects lead to an increasing SSC within the ETM.

Our results also constitute generic findings on the relationship between tidal asymmetry, sediment effects, and ETM dynamics. We observe that the position of the ETM is strongly influenced by the settling velocity (as observed earlier by e.g., de Jonge et al., 2014 and Dijkstra et al., 2019a) but also by sediment-induced effects. We also demonstrate how an estuarine sediment load influences ETM dynamics through sediment-induced turbulence damping (the SedDE). The impact of the SedDE on vertical sediment dynamics has been extensively demonstrated since the work of Winterwerp (2001) and on horizontal transport by Talke et al. (2009); both aspects were integrated by Zhu, van Maren, et al. (2021). However, this work also investigates the contribution of highly concentrated benthic suspensions to ETM dynamics. Although this has been done before for a coastal ETM (van Maren et al., 2020), this study additionally reveals how these highly concentrated near-bed layers influence ETM dynamics for various types of tidal asymmetry.

Another generic result is that our model suggests that higher near-bed SSC achieved by decreasing α leads to a change in the relative role of tidal pumping and estuarine circulation, particularly increasing the contribution of estuarine circulation to landward sediment transport. This effect may be important in understanding sediment transport mechanisms in highly turbid estuaries with strong river and tidal forcing. In these estuaries, the predominance of estuarine circulation or tidal pumping as the main up-estuary transport component is often considered to be related to the magnitude of the tidal range compared to the freshwater flow (Dyer, 1986). Our results

additionally emphasize the important role of sediments in regulating these sediment transport mechanisms, which is important to understand the responses of sediment concentrations to external natural and human-induced forcing (e.g., channel deepening or a change in sediment supply).

It should be highlighted that the methodology to generate the highly concentrated near-bed layer (a reduced deposition factor parameterizing the contribution of consolidation and resuspension, flocculation, and hindered settling) is strongly simplified and needs to be further investigated as part of future research. Our findings should therefore be interpreted in a qualitative sense (in terms of relevant mechanisms such as a landward shift of the ETM by sediment-induced effects) rather than in absolute terms (e.g., the relative importance of reduced deposition vs. tidal asymmetry). Also, the role of the near-bed, highly concentrated suspensions on ETM dynamics should be investigated in more detail for other turbid estuaries as well to validate the concepts presented here.

5. Conclusions

Using a schematized model reflecting the dynamics of the Yangtze Estuary, we explored the roles of tidal asymmetries, sediment properties (critical shear stress and settling velocity), sediment-induced density effects, and high near-bed SSC due to water-bed exchange processes on ETM dynamics. Our model results suggest that the critical shear stress for erosion mainly influences the magnitude of the maximum SSC of the ETM and slightly influences its location, whereas the settling velocity influences the location and strength of the ETM. For fine sediment with a settling velocity of 2 mm/s, the landward migration of the ETM is strongly enhanced by sediment-induced density effects, and more for asymmetric tides with HW slack tide asymmetry than for peak flood tidal asymmetry.

Without sediment-induced density effects, estuarine circulation leads to up-estuary sediment transport for all types of tidal asymmetry, whereas the net landward sediment transport due to tidal pumping is controlled by the type of tidal asymmetry. With sediment-induced density effects, the contribution of estuarine circulation is always strengthened but tidal pumping may be enhanced or weakened depending on the type of tidal asymmetry. Higher near-bed SSC due to water-bed exchange processes additionally strengthens the sediment-induced density gradients due to the enhanced vertical SSC gradients. This effect strongly increases the contribution of estuarine circulation relative to tidal pumping on landward sediment transport, leading to significant landward ETM migration. The enhanced estuarine circulation is closely related to the positive feedback between sediments and salinity. Therefore, our study suggests that sediment-induced effects (density effects and water-bed exchange processes) interacting with tidal asymmetries strongly influence ETM strength and location, which is essential for understanding and interpreting ETM formation mechanisms in future studies.

Data Availability Statement

Data in this study are publicly available at <https://figshare.com/s/71ee46896a66131309cc>.

Acknowledgments

This paper is a product of the project “Coping with deltas in transition” within the Programme of Strategic Scientific Alliances between China and the Netherlands (PSA), financed by the Chinese Ministry of Science and Technology (MOST), Project no. 2016YFE0133700, and Royal Netherlands Academy of Arts and Sciences (KNAW), Project no. PSA-SA-E-02. It was also financially supported by NSFC (Nos. 51739005, U2040216, 41876091) and Shanghai Committee of Science and Technology (Nos. 19QA1402900; 20DZ1204700). C. Zhu is partially supported by the China Scholarship Council (No. 201506140037). Many thanks to Dr. Yoeri Dijkstra and an anonymous reviewer for their constructive comments and suggestions.

References

- Brenon, I., & Le Hir, P. (1999). Modelling the turbidity maximum in the Seine estuary (France): Identification of formation processes. *Estuarine, Coastal and Shelf Science*, 49(4), 525–544. <https://doi.org/10.1006/ecss.1999.0514>
- Burchard, H., Schuttelaars, H. M., & Ralston, D. K. (2018). Sediment trapping in estuaries. *Annual Review of Marine Science*, 10, 371–395. <https://doi.org/10.1146/annurev-marine-010816-060535>
- Cheng, P., Li, M., & Li, Y. (2013). Generation of an estuarine sediment plume by a tropical storm. *Journal of Geophysical Research: Oceans*, 118(2), 856–868. <https://doi.org/10.1002/jgrc.20070>
- Chernetsky, A. S., Schuttelaars, H. M., & Talke, S. A. (2010). The effect of tidal asymmetry and temporal settling lag on sediment trapping in tidal estuaries. *Ocean Dynamics*, 60(5), 1219–1241. <https://doi.org/10.1007/s10236-010-0329-8>
- de Jonge, V. N., Schuttelaars, H. M., van Beusekom, J. E. E., Talke, S. A., & de Swart, H. E. (2014). The influence of channel deepening on estuarine turbidity levels and dynamics, as exemplified by the Ems estuary. *Estuarine, Coastal and Shelf Science*, 139, 46–59. <https://doi.org/10.1016/j.ecss.2013.12.030>
- Dijkstra, Y. M., Schuttelaars, H. M., & Schramkowski, G. P. (2019a). Can the Scheldt river estuary become hyperturbid? *Ocean Dynamics*, 69(7), 809–827. <https://doi.org/10.1007/s10236-019-01277-z>
- Dijkstra, Y. M., Schuttelaars, H. M., & Schramkowski, G. P. (2019b). A regime shift from low to high sediment concentrations in a tide-dominated estuary. *Geophysical Research Letters*, 46(8), 4338–4345. <https://doi.org/10.1029/2019gl082302>
- Dijkstra, Y. M., Schuttelaars, H. M., Schramkowski, G. P., & Brouwer, R. L. (2019). Modeling the transition to high sediment concentrations as a response to channel deepening in the Ems River Estuary. *Journal of Geophysical Research: Oceans*, 124(3), 1578–1594. <https://doi.org/10.1029/2018jc014367>

- Dronkers, J. (1986). Tidal asymmetry and estuarine morphology. *Netherlands Journal of Sea Research*, 20(2–3), 117–131. [https://doi.org/10.1016/0077-7579\(86\)90036-0](https://doi.org/10.1016/0077-7579(86)90036-0)
- Dyer, K. (1986). *Coastal and estuarine sediment dynamics*. John Wiley and Sons. 358.
- Dyer, K. R. (1988). Fine sediment particle transport in estuaries. In *Physical processes in estuaries*, edited, pp. 295–310. Springer. https://doi.org/10.1007/978-3-642-73691-9_16
- Dyer, K. R. (1997). *Estuaries: A physical introduction* (2nd edn). John Wiley Sons. 195.
- Festa, J. F., & Hansen, D. V. (1978). Turbidity maxima in partially mixed estuaries: A two-dimensional numerical model. *Estuarine and Coastal Marine Science*, 7(4), 347–359. [https://doi.org/10.1016/0302-3524\(78\)90087-7](https://doi.org/10.1016/0302-3524(78)90087-7)
- Fettweis, M., Sas, M., & Monbaliu, J. (1998). Seasonal, neap-spring and tidal variation of cohesive sediment concentration in the Scheldt Estuary, Belgium. *Estuarine, Coastal and Shelf Science*, 47(1), 21–36. <https://doi.org/10.1006/eess.1998.0338>
- Friedrichs, C. T. (2011). Tidal flat Morphodynamics. *Tidal flat Morphodynamics* (pp. 137–170). <https://doi.org/10.1016/b978-0-12-374711-2.00307-7>
- Friedrichs, C. T., & Aubrey, D. G. (1988). Non-Linear tidal distortion in shallow well-mixed estuaries—A Synthesis. *Estuarine, Coastal and Shelf Science*, 27(5), 521–545. [https://doi.org/10.1016/0272-7714\(88\)90082-0](https://doi.org/10.1016/0272-7714(88)90082-0)
- Gabioux, M., Vinzon, S. B., & Paiva, A. M. (2005). Tidal propagation over fluid mud layers on the Amazon shelf. *Continental Shelf Research*, 25(1), 113–125. <https://doi.org/10.1016/j.csr.2004.09.001>
- Geyer, W. R. (1993). The importance of suppression of turbulence by stratification on the estuarine turbidity maximum. *Estuaries*, 16(1), 113–125. <https://doi.org/10.2307/1352769>
- Gibson, R., England, G., & Hussey, M. (1967). The theory of one-dimensional consolidation of saturated clays: 1. Finite non-linear consolidation of thin homogeneous layers. *Géotechnique*, 17(3), 261–273. <https://doi.org/10.1680/geot.1967.17.3.261>
- Grasso, F., Verney, R., Le Hir, P., Thouvenin, B., Schulz, E., Kervella, Y., et al. (2018). Suspended sediment dynamics in the Macrotidal seine estuary (France): 1. Numerical modeling of turbidity maximum dynamics. *Journal of Geophysical Research: Oceans*, 123(1), 558–577. <https://doi.org/10.1002/2017jc013185>
- Guo, L., van der Wegen, M., Jay, D. A., Matte, P., Wang, Z. B., Roelvink, D., & He, Q. (2015). River-tide dynamics: Exploration of nonstationary and nonlinear tidal behavior in the Yangtze River estuary. *Journal of Geophysical Research: Oceans*, 120(5), 3499–3521. <https://doi.org/10.1002/2014jc010491>
- Hill, P. S., Voulgaris, G., & Trowbridge, J. H. (2001). Controls on flocculation in a continental shelf bottom boundary layer. *Journal of Geophysical Research*, 106(C5), 9543–9549. <https://doi.org/10.1029/2000jc900102>
- Jalón-Rojas, I., Schmidt, S., & Sottolichio, A. (2015). Turbidity in the fluvial Gironde estuary (southwest France) based on 10-year continuous monitoring: Sensitivity to hydrological conditions. *Hydrology and Earth System Sciences*, 19(6), 2805.
- Jalón-Rojas, I., Schmidt, S., Sottolichio, A., & Bertier, C. (2016). Tracking the turbidity maximum zone in the Loire Estuary (France) based on a long-term, high-resolution and high-frequency monitoring network. *Continental Shelf Research*, 117, 1–11.
- Jalón-Rojas, I., Sottolichio, A., Hanquiez, V., Fort, A., & Schmidt, S. (2018). To what extent multidecadal changes in morphology and fluvial discharge impact tide in a convergent (turbid) tidal river. *Journal of Geophysical Research: Oceans*, 123(5), 3241–3258.
- Jay, D. A., & Musiak, J. D. (1994). Particle trapping in estuarine tidal flows. *Journal of Geophysical Research*, 99(C10), 20445. <https://doi.org/10.1029/94jc00971>
- Jay, D. A., & Musiak, J. D. (1996). *Internal tidal asymmetry in channel flows: Origins and consequences*. (Vol. 50, pp. 211–249). <https://doi.org/10.1029/CE050p0211>
- Jiang, C., de Swart, H. E., Li, J., & Liu, G. (2013). Mechanisms of along-channel sediment transport in the North Passage of the Yangtze estuary and their response to large-scale interventions. *Ocean Dynamics*, 63(2–3), 283–305. <https://doi.org/10.1007/s10236-013-0594-4>
- Kumar, M., Schuttelaars, H. M., & Roos, P. C. (2017). Three-dimensional semi-idealized model for estuarine turbidity maxima in tidally dominated estuaries. *Ocean Modelling*, 113, 1–21. <https://doi.org/10.1016/j.oceamod.2017.03.005>
- Lesser, G. R., Roelvink, J. A., van Kester, J. A. T. M., & Stelling, G. S. (2004). Development and validation of a three-dimensional morphological model. *Coastal Engineering*, 51(8–9), 883–915. <https://doi.org/10.1016/j.coastaleng.2004.07.014>
- Li, J. F., & Zhang, C. (1998). Sediment resuspension and implications for turbidity maximum in the Changjiang estuary. *Marine Geology*, 148(3–4), 117–124. [https://doi.org/10.1016/S0025-3227\(98\)00003-6](https://doi.org/10.1016/S0025-3227(98)00003-6)
- Li, L., He, Z., Xia, Y., & Dou, X. (2018). Dynamics of sediment transport and stratification in Changjiang river estuary, China. *Estuarine, Coastal and Shelf Science*, 213, 1–17. <https://doi.org/10.1016/j.eess.2018.08.002>
- Lin, J., He, Q., Guo, L., van Prooijen, B. C., & Wang, Z. B. (2019). An integrated optic and acoustic (IOA) approach for measuring suspended sediment concentration in highly turbid environments. *Marine Geology*.
- Lin, J., van Prooijen, B. C., Guo, L., Zhu, C., He, Q., & Wang, Z. B. (2021). Regime shifts in the Changjiang (Yangtze River) Estuary: The role of concentrated benthic suspensions. *Marine Geology*, 433, 106403. <https://doi.org/10.1016/j.margeo.2020.106403>
- Liu, G., Zhu, J., Wang, Y., Wu, H., & Wu, J. (2011). Tripod measured residual currents and sediment flux: Impacts on the silting of the deepwater navigation channel in the Changjiang estuary. *Estuarine, Coastal and Shelf Science*, 93(3), 192–201. <https://doi.org/10.1016/j.eess.2010.08.008>
- Lu, S., Tong, C., Lee, D.-Y., Zheng, J., Shen, J., Zhang, W., & Yan, Y. (2015). Propagation of tidal waves up in Yangtze estuary during the dry season. *Journal of Geophysical Research: Oceans*, 120(9), 6445–6473. <https://doi.org/10.1002/2014jc010414>
- Mitchell, S. B., Green, M. O., MacDonald, I. T., & Pritchard, M. (2017). Field studies of estuarine turbidity under different freshwater flow conditions, Kaipara River, New Zealand. *Estuarine, Coastal and Shelf Science*, 198, 542–554. <https://doi.org/10.1016/j.eess.2016.06.009>
- Partheniades, E. (1965). Erosion and deposition of cohesive soils. *Journal of the Hydraulics Division*, 91(1), 105–139. <https://doi.org/10.1061/jyceaj.0001165>
- Postma, H. (1961). Transport and accumulation of suspended matter in the Dutch Wadden Sea. *Netherlands Journal of Sea Research*, 1(1–2), 148–190. [https://doi.org/10.1016/0077-7579\(61\)90004-7](https://doi.org/10.1016/0077-7579(61)90004-7)
- Richardson, J., & Zaki, W. (1954). The sedimentation of a suspension of uniform spheres under conditions of viscous flow. *Chemical Engineering Science*, 3(2), 65–73. [https://doi.org/10.1016/0009-2509\(54\)85015-9](https://doi.org/10.1016/0009-2509(54)85015-9)
- Sanford, L. P., & Halka, J. P. (1993). Assessing the paradigm of mutually exclusive erosion and deposition of mud, with examples from upper Chesapeake Bay. *Marine Geology*, 114(1–2), 37–57. [https://doi.org/10.1016/0025-3227\(93\)90038-w](https://doi.org/10.1016/0025-3227(93)90038-w)
- Sanford, L. P., Suttles, S. E., & Halka, J. P. (2001). Reconsidering the physics of the Chesapeake Bay estuarine turbidity maximum. *Estuaries*, 24(5), 655–669. <https://doi.org/10.2307/1352874>
- Schubel, J. R. (1968). Turbidity maximum of the northern Chesapeake Bay. *Science*, 161(3845), 1013–1015. <https://doi.org/10.1126/science.161.3845.1013>
- Simpson, J. H., Brown, J., Matthews, J., & Allen, G. (1990). Tidal straining, density currents, and stirring in the control of estuarine stratification. *Estuaries*, 13(2), 125–132. <https://doi.org/10.2307/1351581>

- Song, D., Wang, X. H., Cao, Z., & Guan, W. (2013). Suspended sediment transport in the deepwater navigation channel, Yangtze river estuary, China, in the dry season 2009: 1. Observations over spring and neap tidal cycles. *Journal of Geophysical Research: Oceans*, 118(10), 5555–5567. <https://doi.org/10.1002/jgrc.20410>
- Talke, S. A., de Swart, H. E., & Schuttelaars, H. M. (2009). Feedback between residual circulations and sediment distribution in highly turbid estuaries: An analytical model. *Continental Shelf Research*, 29(1), 119–135. <https://doi.org/10.1016/j.csr.2007.09.002>
- Uncles, R., & Stephens, J. (1993). Nature of the turbidity maximum in the Tamar estuary, UK. *Estuarine, Coastal and Shelf Science*, 36(5), 413–431. <https://doi.org/10.1006/ecss.1993.1025>
- Uncles, R. J., Elliott, R. C. A., & Weston, S. A. (1985). Observed fluxes of water, salt and suspended sediment in a partly mixed estuary. *Estuarine, Coastal and Shelf Science*, 20(2), 147–167. [https://doi.org/10.1016/0272-7714\(85\)90035-6](https://doi.org/10.1016/0272-7714(85)90035-6)
- van Kessel, T., & Vanlede, J. (2010). *Impact of harbour basins on mud dynamics Scheldt estuary, the framework of LTV*. Report, 1200253.
- van Maren, D., Vroom, J., Fettweis, M., & Vanlede, J. (2020). Formation of the Zeebrugge coastal turbidity maximum: The role of uncertainty in near-bed exchange processes. *Marine Geology*. <https://doi.org/10.1016/j.margeo.2020.106186>
- van Maren, D., Winterwerp, J., Wang, Z., & Pu, Q. (2009). Suspended sediment dynamics and morphodynamics in the Yellow River, China. *Sedimentology*, 56(3), 785–806. <https://doi.org/10.1111/j.1365-3091.2008.00997.x>
- van Maren, D., Winterwerp, J., Wu, B., & Zhou, J. (2009). Modelling hyperconcentrated flow in the yellow river. *Earth Surface Processes and Landforms*, 34(4), 596–612. <https://doi.org/10.1002/esp.1760>
- van Maren, D. S., Winterwerp, J. C., & Vroom, J. (2015). Fine sediment transport into the hyper-turbid lower Ems river: The role of channel deepening and sediment-induced drag reduction. *Ocean Dynamics*, 65(4), 589–605. <https://doi.org/10.1007/s10236-015-0821-2>
- van Straaten, L., & Kuenen, P. H. (1957). Accumulation of fine grained sediments in the Dutch Wadden Sea. *Netherlands Journal of Geosciences*, 19, 329–354.
- Wan, Y., Gu, F., Wu, H., & Roelvink, D. (2014). Hydrodynamic evolutions at the Yangtze estuary from 1998 to 2009. *Applied Ocean Research*, 47, 291–302. <https://doi.org/10.1016/j.apor.2014.06.009>
- Wan, Y., Roelvink, D., Li, W., Qi, D., & Gu, F. (2014). Observation and modeling of the storm-induced fluid mud dynamics in a muddy-estuarine navigational channel. *Geomorphology*, 217, 23–36. <https://doi.org/10.1016/j.geomorph.2014.03.050>
- Wang, Z. B., Winterwerp, J. C., & He, Q. (2014). Interaction between suspended sediment and tidal amplification in the Guadalquivir Estuary. *Ocean Dynamics*, 64(10), 1487–1498. <https://doi.org/10.1007/s10236-014-0758-x>
- Winterwerp, J. C. (2001). Stratification effects by cohesive and noncohesive sediment. *Journal of Geophysical Research*, 106(C10), 22559–22574. <https://doi.org/10.1029/2000jc000435>
- Winterwerp, J. C. (2011). Fine sediment transport by tidal asymmetry in the high-concentrated Ems river: Indications for a regime shift in response to channel deepening. *Ocean Dynamics*, 61(2–3), 203–215. <https://doi.org/10.1007/s10236-010-0332-0>
- Winterwerp, J. C., Lely, M., & He, Q. (2009). Sediment-induced buoyancy destruction and drag reduction in estuaries. *Ocean Dynamics*, 59(5), 781–791. <https://doi.org/10.1007/s10236-009-0237-y>
- Winterwerp, J. C., & van Kessel, T. (2003). Siltation by sediment-induced density currents. *Ocean Dynamics*, 53(3), 186–196. <https://doi.org/10.1007/s10236-003-0038-7>
- Winterwerp, J. C., van Kessel, T., van Maren, D. S., & van Prooijen, B. C. (2021). *Fine sediment in open water: From fundamentals to modeling*. World Scientific.
- Winterwerp, J. C., & Wang, Z. B. (2013). Man-induced regime shifts in small estuaries—I: Theory. *Ocean Dynamics*, 63(11–12), 1279–1292. <https://doi.org/10.1007/s10236-013-0662-9>
- Yu, Q., Wang, Y. W., Gao, J. H., Gao, S., & Flemming, B. (2014). Turbidity maximum formation in a well-mixed macrotidal estuary: The role of tidal pumping. *Journal of Geophysical Research: Oceans*, 119(11), 7705–7724. <https://doi.org/10.1002/2014jc010228>
- Yun, C. (2004). *Recent development of the Changjiang estuary*. China Ocean Press. (in Chinese with abstract in English). 320.
- Zhu, C., Guo, L., van Maren, D., Wang, Z. B., & He, Q. (2021). Exploration of decadal tidal evolution in response to morphological and sedimentary changes in the Yangtze Estuary. *Journal of Geophysical Research: Oceans*, e2020JC017019. <https://doi.org/10.1029/2020jc017019>
- Zhu, C., van Maren, D. S., Guo, L., Lin, J., He, Q., & Wang, Z. B. (2021). Effects of sediment-induced density gradients on the estuarine turbidity maximum in the Yangtze estuary. *Journal of Geophysical Research: Oceans*. <https://doi.org/10.1029/2020JC016927>

References From the Supporting Information

- Hansen, D. V., & Rattray, M., Jr. (1966). New dimensions in estuary classification 1. *Limnology & Oceanography*, 11(3), 319–326.
- Haralambidou, K., Sylaios, G., & Tsihrintzis, V. A. (2010). Salt-wedge propagation in a Mediterranean micro-tidal river mouth. *Estuarine, Coastal and Shelf Science*, 90(4), 174–184.
- Miles, J. W. (1961). On the stability of Heterogeneous shear flows. *Journal of Fluid Mechanics*, 10(4), 496–508.
- UNESCO. (1981). Background papers and supporting data on the international equation of state 1980. *Technical Report*. (38).